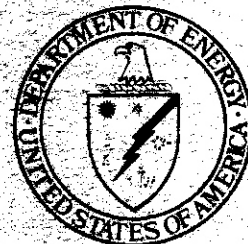


US, mgr, MFE matters, 10-19

DOE/ER-0046/10



Damage Analysis and Fundamental Studies

Quarterly Progress Report
April-June 1982

August 1982

U.S. Department of Energy
Assistant Secretary for Energy Technology
Office of Fusion Energy
Washington, DC 20545

CONTENTS

	<u>Page</u>
Foreword	iii
Figures	xi
Tables	xix

CHAPTER 1: IRRADIATION TEST FACILITIES

1. RTNS-II Irradiations and Operations (LLNL) 3

Irradiations were performed for a total of seventeen different experimenters during this quarter.

After nearly four years of operation, the accelerator tube electron trap failed, causing approximately three weeks of unscheduled outage.

Plans for fabrication of a new accelerator column have begun.

The first U.S.-Japan Steering Committee meeting was held April 19-21 in Tokyo. An initial list of experiments was approved.

CHAPTER 2: DOSIMETRY AND DAMAGE PARAMETERS

1. Dosimetry Results for the TRIO Test in ORR (ANL) 9

Dosimetry was performed for the TRIO tritium recovery experiment in the Oak Ridge Research Reactor (ORR). The tritium production rate from the ${}^6\text{Li}(n,\alpha)$ reaction calculated using the measured flux-spectrum is in excellent agreement with Oak Ridge measurements.

The status of all other dosimetry is summarized in Table I.

2. Experiments at the IPNS Spallation Neutron Source (ANL) 16

Dosimetry results are presented for an irradiation by G. Hurley (LANL) at IPNS (ANL) on February 22-27, 1982 (described elsewhere in this report). The maximum neutron fluence was 1.55×10^{17} n/cm² (>0.1 MeV), 2.23×10^{17} n/cm² (total).

CONTENTS (Cont'd)

	<u>Page</u>
3. <u>Helium Production Cross Sections for 14.8-MeV Neutrons (RIES)</u>	19
<i>Total helium production cross sections for ~14.8-MeV neutrons have been determined for LiF, PbF₂, F, Li, B, the separated isotopes of Li and B, and the three alloys HT-9, 9Cr-1Mo, and Type 316 stainless steel. Some minor alloy constituents are significant contributors. The measured ⁷Li(n,n't)α cross section is ~30% higher than a recent evaluation.</i>	
4. <u>Damage Energy for (n,γ) and Beta-Decay (ANL)</u>	28
<i>Calculation of recoil-atom energy distributions from neutron capture reactions have been revised to take into account the effects of incident neutron energy, gam-ray recoil momentum summing and y-y angular correlations in y-cascades, lifetimes of the intermediate states, and recoil effects resulting from subsequent β-decay when relevant.</i>	
5. <u>Nuclear Data Applications in Radiation Damage Studies (HEDL)</u>	39
<i>The calculated transmutation rate of V-15%Cr-5%Ti is low except in mixed spectrum reactors such as HFIR. The first module of the NJOY code has been successfully modified to handle data in the >20-MeV ENDF/B formats.</i>	
6. <u>A Semi-Empirical Kinetic Model for Quenching of High Energy Displacement Cascades (HEDL)</u>	44
<i>The quenching stage of simulated cascades was accomplished using the stochastic computer code ALSOME with exaggerated values for defect mobilities and critical recombination and clustering reaction distances. Quenching parameter values were chosen to fit experimental defect yields. The number of defect pairs after quenching and after annealing, and the number of freely migrating defects, vary linearly with cascade damage energy from 10 to 100 keV.</i>	

CONTENTS (Cont'd)

	<u>Page</u>
7. <u>Comparison of Neutron and Gamma Irradiation Damage in Organic Insulators (LANL)</u>	53
<i>Three epoxy- and three polyimide-based materials were neutron irradiated in IPNS-1 to an average fluence of 1.51×10^{21} n/cm², $E_n > 0.1$ MeV, at 4.2 K. The gamma dose was less than 15% of the neutron dose (Gy). The environmental and thermal conditions during and after irradiation were similar to those employed in a previous study of gamma irradiation effects at ORNL. Incomplete measurements of mechanical, electrical, and optical properties have disclosed some differences between neutron and gamma effects.</i>	
 CHAPTER 3: <u>FUNDAMENTAL MECHANICAL BEHAVIOR</u>	
1. <u>Correlation of Hardness and Strength Data for High Energy Neutron Irradiated Annealed 316 Stainless Steel (HEDL)</u>	77
<i>Strength values derived from hardness data are in good agreement with actual tensile data for 14-MeV neutron-irradiated annealed 316 stainless steel.</i>	
2. <u>Hardening of Irradiated Alloys Due to the Simultaneous Formation of Vacancy and Interstitial Loops (UCLA and HEDL)</u>	84
<i>A model based on homogeneous time-dependent rate theory is presented for the simultaneous nucleation and growth of vacancy and interstitial loops in irradiated metals.</i> <i>A simple hardening model relating the microstructural calculations to changes in tensile strength gives good agreement with hardening data for copper irradiated in RTNS-11 at room temperature.</i>	
3. <u>A Model for the Evolution of Network Dislocation Density in Irradiated Metals (HEDL and U. of Wisconsin)</u>	106
<i>A literature review shows that the network dislocation density in irradiated metals approaches a saturation level which is relatively</i>	

CONTENTS (Cont'd)

Page

insensitive to starting microstructure, stress, irradiation temperature, displacement rate and helium level. A model, taking into account the correlated nature of dislocation components in a dense array, has been developed to explain this insensitivity.

4. Relationships Between Crack Propagation and Tensile Properties in Type 316 Stainless Steel Foil Microspecimens (U. of Virginia) 130

It has been demonstrated that some tensile data obtained from 40- μm thick foil microspecimens pulled in-situ in an HVEM are related to bulk tensile data. The in-situ data are related to the manner in which the main crack propagates through the thin (<1- μm) regions of the specimen. Statements about specimen ductility may possibly be made from this relationship.

CHAPTER 4: CORRELATION METHODOLOGY

1. Cavity Formation and Solute Segregation in Dual-Ion Irradiated Fe-20Ni-15Cr Alloy (ANL) 145

Swelling of specimens receiving helium deposition rates of 15 or 50 appm He per dpa at 975K tends to achieve a limiting value after ~ 70 dpa. Grain boundaries and voids are increasingly enriched in nickel, with a corresponding depletion of the nickel concentration in the matrix, for increasing displacement damage up to 2.70 dpa. For displacement damage >70 dpa, the nickel enrichment appears to diminish. The change in chromium concentration at the grain boundaries and voids and in the matrix is opposite to the change in nickel concentration and of smaller magnitude.

CONTENTS (Cont'd)

	<u>Page</u>
2. <u>On Radiation-Induced Segregation and the Compositional Dependence of Swelling in Fe-Ni-Cr Alloys (U. of Wisconsin and HEDL)</u>	157
<i>It appears that elemental segregation to void surfaces plays an important role in the development of voids. Previously unconsidered drift terms are shown to arise in the description of the bias as a result of elemental segregation. When compounded with the operation of the inverse Kirkendall segregation mechanism, these terms provide an explanation for the marked variation of void nucleation and swelling with nickel concentration.</i>	
3. <u>The Influence of Cold Work Level, Solute and Helium Content on the Swelling of "Pure" AISI 316 (Fe-17Cr-16.7Ni-2.5Mo) (HEDL)</u>	181
<i>Examination of "pure 316" specimens irradiated to 3-5 dpa in ORR shows that both the volume and density of voids are insensitive to cold work.</i>	
<i>The preinjection of 30 appm helium appears to suppress visible swelling; however, both density change measurements and postirradiation aging studies indicate that swelling may exist in the form of unresolvable cavities.</i>	
4. <u>The Effect of Helium on Swelling in Stainless Steel: Influence of Cavity Density and Morphology (UCSB)</u>	199
<i>Data on irradiated 316 stainless steel suggests that the cavity density scales as $(\text{He}/\text{dpa})^p$, where $0 < p < 1$. A rate theory model, calibrated using data from EBR-11 irradiations of 20% cold worked 316 stainless steel, was used to examine the parametric dependence of cavity swelling on the value of p and the He/dpa ratio. Beyond a critical value of p there is a bifurcation in the cavity evolution path from microstructures dominated by precipitate-associated</i>	

CONTENTS (Cont'd)

Page

voids to microstructure dominated by matrix bubbles. The model predicts peak swelling near the fusion He/dpa ratio suggesting that the use of fission reactor swelling data may lead to non-conservative estimates of swelling for fusion.

5. Microstructural/Microchemical Evolution of AISI 316 Irradiated at Temperatures in the Range 650-750°C (HEDL) 233

Swelling in two specimens irradiated in EBR-II to temperatures of 700-720°C is found to be comparable to that observed at 650°C and below, but the void densities are lower. Voids appear first in grains that have nickel levels below 12-13 wt.%. The matrix content of nickel declines to ~9% as the swelling increases.

6. Lithium Doping of 316 Stainless Steel to Simulate Irradiation Damage in a Fusion Reactor Environment (MIT) 249

Austenitic stainless steel containing a uniform distribution of lithium was prepared using rapid solidification processing and a powder metallurgy salt decomposition technique. The advantage of a lithium dopant is that it produces only helium and hydrogen.